Divalent Cation Adsorption on the Actin Monomer†

Wei Shi,‡ Munish V. Inamdar,§ Ann M. Sastry,§,|| and Christian M. Lastoskie*,‡,||

Departments of Civil and Environmental Engineering, Mechanical Engineering, and Biomedical Engineering, University of Michigan, Ann Arbor, Michigan 48109

Received: May 15, 2007; In Final Form: August 18, 2007

Binding energies for calcium adsorption on the actin monomer have been computed from molecular dynamics simulation using the CHARMM22 force field. Relative binding free energies were evaluated from Poisson−Boltzmann computations. For large values of the dielectric constant (i.e., > 4), binding affinity is highest at the adsorption site near the nucleotide in the cleft region of the monomer, and the binding free energies of five other calcium adsorption sites are statistically comparable. For small values of the dielectric constant (i.e., unity) for the ion−protein complex, all six binding sites exhibit comparable binding affinity. Replacing the ADP nucleotide with ATP has only a small effect on the binding potential energy change for calcium at the six crystallographic adsorption sites. Likewise, the presence of charged residues at the N-terminus of the monomer only modestly affects the binding potential energy at the crystallographic calcium sites. Molecular simulation snapshots reveal that calcium ions at the cystallographic sites are coordinated by one or two acidic side chains and three or four water molecules. Free energy perturbation methods were used to compute the selectivity between zinc and calcium ion binding in the cleft region. In the cleft region, the exchange of bound Zn^{2+} for bound Ca^{2+} incurs a free energy change of −12.3 (3.4) kcal/mol for solvated actin. This agrees with experimental observations that calcium exhibits a higher binding affinity than zinc at the primary divalent cation binding site of the actin monomer.

1. Introduction

Actin is a highly conserved, dynamic polymerizing protein found in the cytoplasm of all eukaryotic cells. The filamentous form of self-assembled actin, referred to as F-actin, carries out important functions in cellular locomotion and intracellular transport. At neutral pH and in the presence of free magnesium, actin monomers assemble into twin right-handed helical filaments approximately 10 nm in diameter with a half-pitch of 36 nm per 13 monomers.[1] Filament structure parameters have been determined from X-ray diffraction measurements[2] and fluorescence resonance energy transfer spectroscopy.[3] F-actin organizes into a wide variety of cytoskeletal structures through binding with gelsolin and α-actinin proteins that bundle and network filaments.[4,5]

The crystal structures of the actin monomer, also known as globular or G-actin, and complexes of actin with various binding proteins have been reported.[6−9] As shown in Figure 1, G-actin is cubic in shape with a side length of about 5.5 nm and a thickness of 3.5 nm. It is composed of 375 ± 1 amino acid residues, divided into two domains connected by a covalently bonded hinge of two chain strands.[1] The N- and C-termini of the protein are located in the smaller domain I, whereas in the F-actin structure each monomer unit is oriented so that its domain II is positioned closer to the filament axis.

It has been established that actin possesses a high affinity site, located in the cleft of the monomer, that strongly binds calcium, with a dissociation equilibrium constant K_d in the nanomolar range.[10,11] Experimental studies have also revealed the presence of three or four calcium binding sites of intermediate affinity, and multiple calcium sites of low affinity, that have K_d values in the 10^{-4} molar and 10^{-2} molar range, respectively.[12]

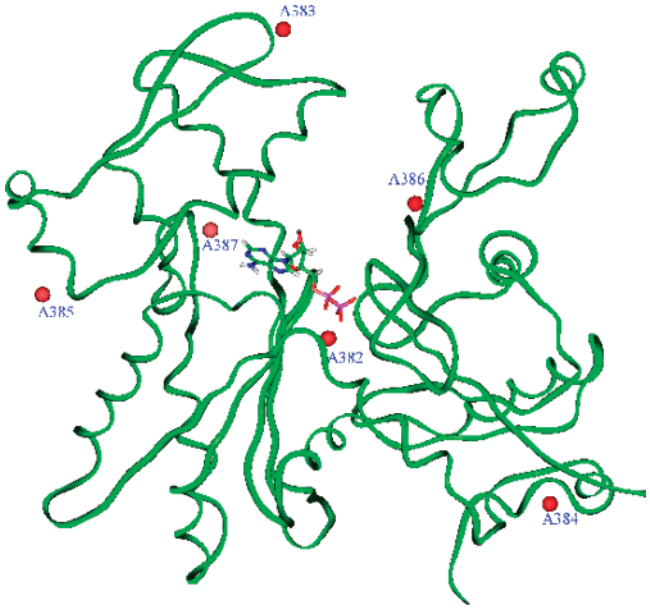

Figure 1. Ribbon structure of the energy-minimized actin monomer. The positions of the six crystallographic calcium binding sites, labeled CA382−CA387, are shown as the red spheres. The position of the ADP nucleotide near CA382 is denoted in stick format. For clarity, the intracrystalline water is not shown.

The principal function of the tightly bound cation at the high-affinity site is to stabilize actin monomer in its complex with ATP, which binds the cation in the monomer cleft and whose

† Part of the "Keith E. Gubbins Festschrift".
* Corresponding author. e-mail: cmlasto@umich.edu.
‡ Department of Civil and Environmental Engineering.
§ Department of Mechanical Engineering.
|| Department of Biomedical Engineering.

10.1021/jp073763i CCC: $37.00
Published on Web 10/10/2007

hydrolysis accompanies the polymerization of monomer units into filaments. If the high-affinity site is not occupied by a divalent cation, then the nucleotide rapidly dissociates and the actin monomer denatures.[10] In vivo, the tightly bound cation site is occupied by magnesium, rather than calcium, because of the much higher cellular concentration of free magnesium; however, all cation binding sites on the monomer, including the high-affinity site, are exchangeable with other divalent ions.[13,14] The selectivity trends among cations for the actin affinity sites do not follow a predictable order. Nickel, for example, selects poorly for the high-affinity site on G-actin, but it outcompetes other divalents at the low-affinity sites.[15] The lower-affinity sites, meanwhile, do not discriminate between calcium and magnesium, and bind monovalent cations such as potassium.[16] Interestingly, zinc binds at the high-affinity calcium site, and at two other undetermined sites of high affinity that exclude other divalent cations.[17]

Saturation of the high- and intermediate-affinity divalent cation binding sites of actin promotes polymerization by reducing repulsion between negatively charged monomers.[18] Stoichiometric observations indicate that a ratio of five divalent cations per monomer is required to sufficiently overcome monomer−monomer charge repulsion and form filaments. Although their importance has thus been established, the locations of the intermediate-affinity divalent cation binding sites on the actin monomer have yet to be conclusively determined. In this paper, the results of molecular simulations of the binding site coordination, energetics, and free energy are reported for six putative calcium binding sites on the actin monomer. Also, the effects of nucleotide substitution, N-terminal loop alignment, and solvation on the binding energies are noted.

In the remainder of this paper, the following abbreviations appear frequently and are summarized here for reference: ADP = adenosine diphosphate; ATP = adenosine triphosphate; PDB = Protein Data Bank; MD = molecular dynamics; vdW = van der Waals; RMSD = root mean square deviation; PBCs = periodic boundary conditions.

2. Methods

2.1. Construction of the Model System. The atomic coordinates of the actin monomer were obtained from the X-ray crystallographic structure reported for uncomplexed actin in the RCSB protein data bank (1J6Z)[9]. Other actin coordinate sets have been reposited in the PDB,[7,8] and some of these have been used in molecular simulation studies of actin conformational changes.[19,20] However, in these other structures actin is complexed with various binding proteins, and hence these coordinate sets were deemed less desirable in the context of the present study. Additionally, in the ATP-bound actin structure reposited by Kabsch et al. (1ATN), only one calcium binding site is reported, and no intracrystalline water molecules are noted. In contrast, the positions of six calcium ions, the ADP nucleotide, and 404 intracrystalline water molecules are identified, at higher resolution, in the 1J6Z PDB structure for uncomplexed actin.

Because of low electron density in the crystallographic measurement, three residues on the N-terminal end and three residues on the C-terminal end are missing from the 1J6Z actin PDB structure. Several atoms are also missing from residue 4 of this structure. The missing atoms and residues for 1−4 in 1J6Z were reconstructed using atomic coordinates for residues 1−4 in 1ATN by superimposition. The residues for 373−375 in 1J6Z were added using the "extended" method in Insight II. The superimposition was accomplished by translating the center of mass of 1J6Z a distance x_0, y_0, and z_0 in x-, y-, and z-coordinate directions, respectively, and rotating 1J6Z an angle α, β, and γ around the x-, y-, and z-axes, respectively, with the values of x_0, y_0, z_0, α, β, and γ selected so as to minimize the difference in alignment between the 1J6Z and 1ATN structures as measured by the root mean square distance between all corresponding atoms of residues 4−372. Once the optimal alignment is found, the missing residues were pruned from 1ATN and grafted onto 1J6Z.

The fluorescent probe molecule tetramethylrhodamine-5-maleimide, which was used to crystallize the uncomplexed actin monomer, was removed from the structure so that only the monomer, ADP, intracrystalline water and six calcium ions were retained for the molecular dynamics (MD) simulations. Hydrogen atoms were added to the heavy atoms of the protein, and a net charge of +1 was assigned to histidine residues 88, 101, 275, and 371, based on the stabilization of these residues by nearby hydroxyl or carboxyl groups.[19] The methylated histidine residue 73 was also protonated. This residue has been shown to play a significant role in the structure of the cleft region of the monomer.[20] In the 1J6Z actin monomer, the N-terminus is acetylated and hence is uncharged, whereas the C-terminus bears a charge of −1.

At neutral pH, the negative charges of 50 glutamic and aspartic acid residues, the C-terminal residue, and the ADP nucleotide (−3) are offset by the positive charges of 42 lysine, arginine, histidine, and methylhistidine residues, yielding a net charge of −12 for ADP-bound actin. Hence, six divalent cations are required to achieve charge neutrality. The six calcium ions, initially assigned to their 1J6Z PDB crystallographic coordinates, provide the charge balance desired for the molecular simulations. To distinguish between these six calcium binding sites, their locations are henceforth referred to as CA382−CA387, as shown in Figure 1, where the indices assigned to the calcium heteroatoms in the 1J6Z PDB file have been adopted.

2.2. Simulation Methodology. Initial energy minimization was carried out sequentially, first for the appended residues from the 1ATN structure, then for the missing residues from 373 to 375, followed by the hydrogen atoms, the intracrystalline water molecules, and the entire system of 7095 atoms comprising the full reconstructed actin monomer, ADP, intracrystalline water, and six calcium ions. The CHARMm all-hydrogen force field (version 22) was utilized[21] with the TIP3 potential[22] employed for explicit water molecules. A dielectric constant of 1 was used. Approximately 5000 minimization steps were carried out. The system at the conclusion of the energy minimization procedure is shown in Figure 1. All six calcium ions remain in positions near their coordinates reported in the 1J6Z PDB structure. This is the calculation in vacuo. Simulations in solvated system described below have been performed in a similar way as in vacuo.

Following energy minimization, MD simulations were carried out to assess the impact of certain structural features of the actin−nucleotide complex on the calcium interaction energies. Because the purpose of these calculations is to evaluate the sensitivity of the calcium potential energies to the assumed structure of their protein environment, the simulations were carried for expediency in vacuum; that is, neither solvent water nor periodic boundary conditions were utilized. The energy-minimized system was heated in 5 ps from 240 to 300 K. An equilibration period of 215 ps was then followed by a production run of 210 ps. A time step of 0.001 ps was employed, and the switch potential was used for both the van der Waals (vdW) and electrostatic portions of the force field, with "on" and "off" distances of 11 and 14 Å used, respectively, as the cutoffs of

the switching function. Neighbor lists were constructed to a distance of 15 Å. The system temperature was rescaled at 0.05-ps intervals during equilibration. The temperature window is set to be between 290 and 310 K. The total energy was well conserved, save for a one-time decrease of 3.9% that occurred during the equilibration period at 112 ps when the velocities of the atoms were rescaled so as to decrease the temperature of the system from 308.8 to 295.9 K. This was necessary in order to remove the heat input into the kinetic energy of the atoms as the potential energy of the system decreased during the equilibration stage. In this manner, the system was thermostatted successfully near the desired set point temperature of 300 K.

Conformational changes of the protein and its ligands during the simulation are monitored by calculating the root mean square deviation (RMSD) between two conformations at the beginning and end of a specified time interval. To account for possible translational or rotational drift of the entire system during the time interval, superposition of the initial and final configurations using the aforementioned alignment procedure is carried out so as to produce the lowest possible RMSD between these two structures. The RMSD is given as

$$\mathrm{RMSD} = \left[\sum_{i=1}^{n} (r_i - r_{i\,0})^2/n\right]^{1/2} \qquad (1)$$

where r_i and r_{i0} are the atomic coordinates at the end and the beginning of the time interval, respectively, and the summation is taken over the set of n heavy atoms consisting of the calcium ions, the water oxygens, and the non-hydrogen atoms of ADP and actin residues 4−372.

Additional MD simulations were performed in which the ADP nucleotide and its associated calcium ion in the 1J6Z actin PDB structure were replaced with the ATP nucleotide and its adjacent calcium ion pruned from the 1ATN PDB structure. The substitution was made using the superposition procedure. Energy minimization, heating to 300 K, and MD equilibration for 100 ps were then followed by a production run of 100 ps for the ATP−actin system.

2.3. Solvation of the Actin Monomer. To investigate the effect of solvation of actin on the binding energies of calcium ions, the protein was solvated with 3502 additional water molecules to form a droplet of 10 Å thickness encapsulating the monomer. Energy minimization was then carried out on the solvated protein system of 17 601 atoms, followed by heating to 300 K, MD equilibration for 1 ns, and property collection for 300 ps. All simulation parameters and potentials for the solvated system were otherwise the same as for the in vacuo system. The MD calculations were repeated using an actin monomer solvated with 5198 water molecules, thereby increasing the water droplet thickness of 15 Å to allow evaluation of the effect of the water layer thickness on the calcium binding energies. For this larger system of 22 689 total atoms, minimization and heating were followed by short MD equilibration and production runs each 100 ps in duration.

In the aforementioned MD simulations, electrostatic interactions between atoms were simply truncated. To evaluate the effect of long-range calcium ion pair repulsion on calcium ion binding, an extended electrostatics model was implemented.[23] MD calculations for the actin monomer with a 10 Å solvation water layer were repeated using the extended electrostatics model in which interactions between spatially distant atom pairs beyond a cutoff distance of 14 Å were included using a multipole approximation. The extended electrostatics model was evaluated by comparing the total potential energy for a number of snapshots of the solvated system with the potential energy from the full vdW and electrostatic interactions obtained when extremely large cutoff values are used for the "on" and "off" values of the switch potential (490 and 499 Å, respectively). The difference in the total potential energy for the two force fields is very small, less than 0.3%. Hence, the extended electrostatics model was judged to give a suitable representation of the potential energy of the solvated monomer.

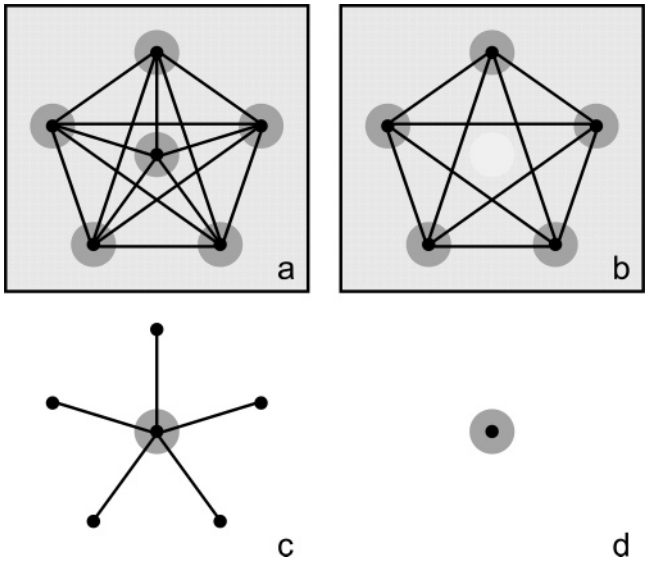

Figure 2. Schematic of annihilation procedure used to calculate binding energies for calcium adsorption. Potential energies are computed from configurational sampling via molecular dynamics simulation of the system shown in part a, which is comprised of six calcium ions (dark circles), the actin monomer, the ADP nucleotide, intracrystalline water, and solvent water. The shaded regions around each calcium ion represent its interactions with the protein, nucleotide, and water. The light-shaded region enclosed by the square represents the potential energy sum of the system interactions that do not involve the calcium ions (protein−protein, protein−ADP, protein−water, ADP−ADP, ADP−water, and water−water). The lines represent electrostatic repulsion between pairs of calcium ions. Details of the annihilation procedure depicted in parts b−d for the binding energy calculation are provided in the text.

The solvated system was equilibrated for 300 ps at 300 K, with property sampling following for a 700-ps interval. The potential energy change for calcium ion binding at each affinity site was calculated using the annihilation procedure for the thermodynamic cycle[24] as shown schematically in Figure 2. Configurational sampling of the system of protein, solvent, ADP, intracrystalline water, and six calcium ions, represented in Figure 2a, was carried out using MD simulation. After each prescribed interval of time steps, one of the six calcium ions is deleted, yielding the system shown in Figure 2b. The potential energy difference $E_b - E_a$ is calculated between this system and the full system of Figure 2a. This calculation is repeated for the other five calcium ions as each is deleted in turn. The computed difference, Figure 2c, represents the potential energy increase when a bound calcium ion is removed from the fully loaded protein, with the attendant loss of its interactions with the actin monomer, ADP, solvent, intracrystalline water, and other calcium ions. The ensemble average of the negative of this difference, $\Delta E = \langle E_a - E_b \rangle_a$, is the potential energy decrease that occurs when a sixth calcium ion adsorbs onto a monomer that is already bound with five other calcium ions.

Ensemble-averaged values of ΔE are reported for calcium binding with calcium ion pair repulsions excluded, as shown schematically in Figure 2d. As noted later, these values are

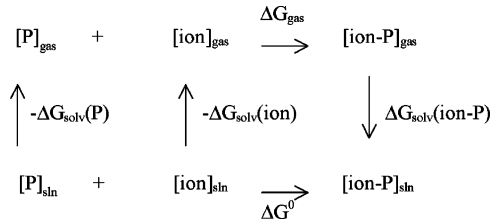

Figure 3. Schematic of the thermodynamic cycle used to calculate the binding free energy for calcium ion adsorption on the actin monomer. "P", "gas", and "sln" denote the protein, vacuum, and solution phase, respectively.

reported to provide a qualitative comparison of calcium binding energies at low calcium loadings.

2.4. Binding Free Energies. The relative binding free energy was computed from the Poisson−Boltzmann equation. The thermodynamic cycle shown schematically in Figure 3 was used to compute the binding free energy of an ion on the protein, using a similar scheme as Lim et al.[25] The binding free energy in solution is given as

$$\Delta G^0 = \Delta G_{\text{gas}} + \Delta G_{\text{solv}}(\text{ion-P}) - \Delta G_{\text{solv}}(\text{P}) - \Delta G_{\text{solv}}(\text{ion}) \quad (2)$$

To determine the relative affinity of calcium ions on different protein binding sites, we calculated only ΔG_{gas} and ΔG_{solv}(ion-P). The desolvation free energies of the calcium ions and the unbound protein are identical for all sites and were therefore excluded. The solvation free energy of ΔG_{solv}(ion-P) is due to the nonpolar (cavity/vdW) energy and the electrostatic ($\Delta G_{\text{solv}}^{\text{elec}}$) energy contributions. The nonpolar energy contribution is assumed to be the same for all six ion−protein complexes, each with a single ion binding on a different binding site. The electrostatic energy contribution was computed using the finite difference Poisson−Boltzmann equation[26,27] with the PBEQ module in CHARMM[21]. A grid spacing of 0.4 Å was used, with a margin of at least 6 Å imposed from the boundary of the protein to the edge of the grid so as to avoid boundary effects. The boundary between the solute (i.e., the protein) and the solvent was mapped by rolling a solvent-sized probe over the van der Waals surface of the solute. The radius of the probe in the vacuum and in solution was chosen according to the value adopted for the dielectric constant. For a dielectric constant of unity (i.e., no protein polarizability), the probe radii are set to zero and 1.4 Å in vacuum and in solution, respectively. For a polarizable protein with a dielectric constant greater than unity, a probe radius of 1.4 Å was used both in vacuum and in solution. Values of the dielectric constant ranging from unity (for a vacuum) and 80 (for room-temperature water) were considered for the continuum representation of the solvent. The van der Waals radii and atomic charges of the solute were taken from the CHARMM22 force field, and the ionic strength was set to zero. This reduced form of the Poisson−Boltzmann equation yields the simple Poisson equation.

The gas-phase binding free energy, ΔG_{gas}, is given by

$$\Delta G_{\text{gas}} = \Delta E_{\text{gas}} + p\Delta V - T(\Delta S^{\text{trans}} + \Delta S^{\text{rot}} + \Delta S^{\text{vib}} + \Delta S^{\text{conf}}) \quad (3)$$

where ΔE_{gas} is the sum of the van der Waals and electrostatic interactions between a calcium ion and the protein unbound with other calcium ions. The second and third terms on the right-hand side of eq 3 are assumed to be similar for the six binding sites and therefore are not included in the calculation. ΔE_{gas} was computed using the CHARMM22 all-hydrogen force field, with no truncation or shift, and with a large cutoff value (490 Å) so as to explicitly include all van der Waals and electrostatic interactions between the calcium ion and the unbound protein. The dielectric constant was set to unity. Trajectories from MD simulation were used to evaluate ΔG_{solv}(ion-P) and ΔE_{gas}.

2.5. Effects of Periodicity. All MD simulations of the solvated protein were performed without using periodic boundary conditions (PBCs). The effect of periodic boundaries on calcium ion binding were considered using a simulation cell of dimension 87 × 71 × 63 Å^3. A cell of this size allows for a solvent layer of 10-Å thickness between the protein and the nearest periodic image in each of the Cartesian coordinate directions. The total number of atoms in the periodic system is 38 361. Electrostatic interactions were calculated via the particle mesh Ewald summation[29] using a real space cutoff distance of 10 Å, screening parameter $\kappa = 0.32$ Å^{-1}, a grid density of 1 Å, and a fifth-order polynomial spline for interpolation between grid points. The crystal module in the CHARMM program was used to construct the PBCs. The vdW interactions were calculated using the switch method with "on" and "off" distances of 8 and 10 Å, respectively. The neighbor list for the periodic images was constructed using a distance cutoff of 11 Å. MD simulations were carried out using a time step of 0.001 ps for 200 ps equilibration and a production run of 420 ps, following minimization and heating.

Trajectories from all MD calculations were analyzed to calculate the potential energies between the calcium ion(s) and all other constituents of the model system. Large cutoff values for the vdW and electrostatic interactions were used (i.e., energies were explicitly summed to an interatomic distance of 490 Å) so that truncation errors were not introduced into the reported energies.

2.6. Cation Substitution. Free energy perturbation was used to compute the free energy of the cation exchange reaction $Ca^{2+} + Zn^{2+}$−actin → $Zn^{2+} + Ca^{2+}$−actin. The reaction free energy was calculated as the sum of the free energy changes that occur when solvated Ca^{2+} is transformed into solvated Zn^{2+}, and when the solvated Zn^{2+}−actin complex is transformed into the solvated Ca^{2+}−actin complex. The free energy change of the transformation from unbound Ca^{2+} to unbound Zn^{2+} in solution was estimated from the experimental solvation free energies of −482.5 and −380.8 kcal/mol, respectively, for zinc and calcium.[30−32] The free energy change of the transformation Zn^{2+}−actin → Ca^{2+}−actin was computed by perturbation, wherein one calcium ion (e.g., the bound ion at the CA382 site) is "alchemically" transformed into a zinc ion by incrementally changing its van der Waals radius, while the other five calcium ions remain unmodified. Assigning λ as the perturbation parameter, with $\lambda = 0$ and $\lambda = 1$ corresponding to a zinc ion and a calcium ion, respectively, free energy perturbation was carried out for increments $\Delta\lambda = 0.1$, using the van der Waals radii for zinc and calcium of 1.09 and 1.71 Å, respectively, and the van der Waals well depths for zinc and calcium of −0.25 and −0.12 kcal/mol, respectively, obtained from the CHARMM22 force field. For each value of λ between 0 and 1, a 5-ps MD equilibration and 10-ps production run was performed, with the atomic coordinates and momenta at the end of the production run for a perturbation parameter of λ_i serving as the initial configuration for the equilibration of the system with perturbation parameter $\lambda_{i+1} = \lambda_i + \Delta\lambda$. The initial structure for the Zn^{2+}−actin simulation is constructed from the 1J6Z actin PDB structure by replacing the crystallographic calcium ions with zinc ions. The Zn^{2+}−actin system was subjected to 5-ps heating

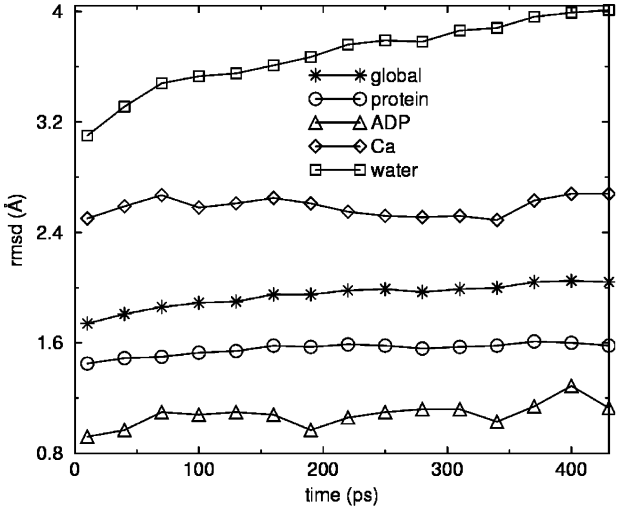

Figure 4. Calculated RMSD values versus simulation time for the (a) unsolvated and (b) solvated actin−ADP system with six bound calcium ions, with initial positions at the crystallographic 1J6Z PDB coordinates. In addition to the global RMSD, RMSDs are shown for the subsets of the calcium ions, ADP, intracrystalline water, and residues 4−372 of the protein. The RMSD is reported for each set relative to the initial positions of its constituents in the 1J6Z actin PDB structure. Hydrogen atoms are excluded from the RMSD calculations. The first data point for each set shows the RMSD at the end of the minimization stage.

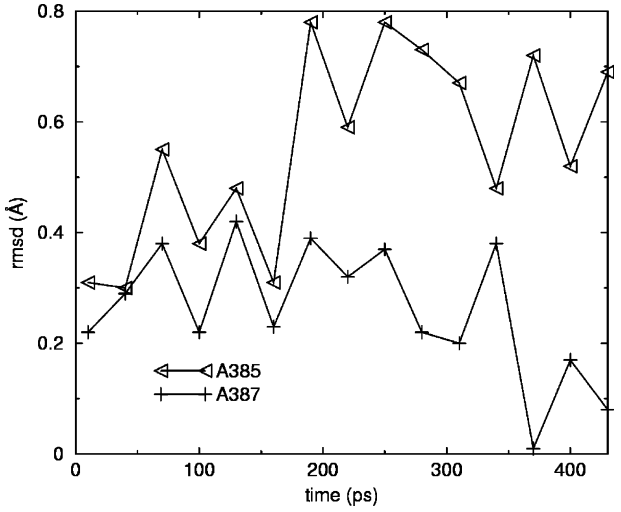

Figure 5. RMSD values for calcium ions at two binding sites, CA385 and CA387, over the course of in vacuo MD simulation of the actin−ADP system. The RMSD values for calcium ions at the other actin binding sites (CA382, CA383, CA384, and CA386) are bracketed by the RMSDs for CA385 and CA387, and for clarity they are not shown.

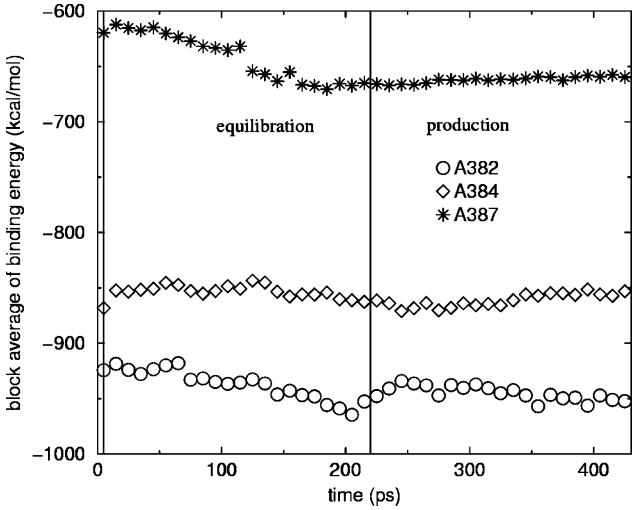

Figure 6. Block-averaged binding energies for calcium ions at three binding sites, CA382, CA384, and CA387, computed at 10-ps intervals for the unsolvated actin−ADP system. The completion of the equilibration period and onset of the production run is indicated. The block-averaged binding energies for calcium ions at the other actin binding sites (CA383, CA385, and CA386) lie intermediate between the curves for CA384 and CA387, and for clarity they are not shown.

and 80-ps equilibration prior to the production run. When the reverse transformations from calcium to zinc were performed, the initial atomic coordinates and momenta were assigned from the configuration at the conclusion of the zinc to calcium transformation.

All MD simulations were performed on a 3-node, 12-processor SunFire V480 cluster. Visualization and binding site analysis was carried out using the Insight II life sciences modeling environment (Accelrys) on a SiliconGraphics O2 workstation.

3. Results

3.1. Root Mean Squared Displacements. The conformational evolution of the in vacuo actin−ADP system is indicated by the global and subset RMSDs shown in Figure 4a. Relative to the initial atomic coordinates of the 1J6Z actin PDB structure, the RMSDs for the protein, ADP, and calcium converge to about 1.5, 1.0, and 2.5 Å, respectively. At the end of the energy minimization, the global RMSD is 1.68 Å. Most of the increase in the global RMSD that occurs thereafter may be attributed to an RMSD increase of intracrystalline water, which is projected to surpass 4 Å if the MD simulation were extended beyond 425 ps. The larger RMSD for intracrystalline water is not surprising given that small, uncharged water molecules are more mobile than the protein, ADP, or tightly bound calcium ions.

The mean displacement for the six ions during the minimization stage is 2.5 Å. The calcium ions at locations CA383 and CA384 experience larger displacements (RMSDs of 4.16 and 3.29, respectively) than the other calcium ions. These particular calcium ions are bound at sites near the monomer surface, and their larger mobility may in part be attributable to the absence of solvent water in this simulation.

RMSDs during MD equilibration and production phases are shown for two of the six calcium ions in Figure 5. The variation in the potential energy between one ion and other atoms in the

TABLE 1: Potential Energy Change ΔE Obtained from MD Simulation for Calcium Binding on the Actin Monomer for Different Combinations of Solvation Layer Thickness, Bound Nucleotide, and Construction Method for the Missing N-terminal Region of 1J6Z Actin[a]

	ΔE (kcal/mol)					
solvent layer (Å)	none	none	none	none	10	15
nucleotide	ADP	ADP	ATP	ADP	ADP	ADP
N-terminus	1ATN	extended	1ATN	1ATN	1ATN	1ATN
Ca-Ca repulsion	yes	yes	yes	no	no	no
CA382	−669	−675	−704	−941	−911	−925
	(19)	(16)	(16)	(19)	(16)	(17)
CA383	−562	−577	−589	−773	−773	−763
	(14)	(14)	(15)	(15)	(15)	(15)
CA384	−725	−692	−680	−893	−774	−751
	(13)	(13)	(11)	(13)	(15)	(15)
CA385	−542	−544	−572	−744	−750	−734
	(15)	(13)	(17)	(15)	(17)	(16)
CA386	−549	−555	−540	−803	−801	−722
	(14)	(13)	(14)	(14)	(14)	(14)
CA387	−424	−432	−427	−655	−768	−785
	(9)	(10)	(9)	(9)	(16)	(17)

[a] Inclusion or neglect of calcium−calcium repulsion in the energy calculation is also noted. Standard deviations for the reported values are enclosed in parentheses.

system for three of the six calcium ions (excluding calcium−calcium interactions) is shown over the course of the simulation in Figure 6. The small RMSD values in Figure 5 indicate that the ions are tightly constrained to the regions near the crystallographic binding sites. Moreover, the RMSD of the calcium ions for the entire MD simulation was observed to be much smaller than the displacement incurred during the energy minimization.

3.2. Binding Potential Energies. The potential energies of the calcium ions fluctuate around equilibrium values established after approximately 150 ps (Figure 6). From Figure 4a, it is evident from the increasing global RMSD that the potential energy of the full system of actin, ADP, intracrystalline water, and calcium ions may yet undergo an additional slight decrease, principally by reordering of intracrystalline water. However, Figures 5 and 6 show that calcium ions are localized at specific binding sites, and that within these regions their binding energies are effectively minimized. Extending the length of the MD simulation may thus accomplish small reductions in the global energy of the system, but it is unlikely to dramatically affect the energies of the bound calcium ions. Longer, 3-ns MD simulations of the solvated actin monomer were performed that confirm this expectation. Hence, the binding energies of the calcium ions may be estimated accurately from shorter MD simulations of the duration shown in Figures 4−6.

The binding potential energies of the calcium ions, calculated per Figure 2c, are reported for the unsolvated actin−ADP system and other related systems in Table 1. For the unsolvated monomer, two binding sites, CA382 and CA384, have distinctly higher binding potential energies than the other sites, and one site, CA387, is noticeably weaker in its calcium binding energy. The effect of the reconstruction procedure used to append the missing residues to the terminal ends of the 1J6Z actin structure is shown in Table 1 with the comparison of the "1ATN" and "extended" N-terminal configurations. In the latter configuration, the missing residues 1−3 are appended in the extended alignment using the Insight II model builder, rather than by attachment of the corresponding residues pruned from the 1ATN PDB file. The extended conformation yields a markedly different initial structure than the 1ATN conformation: prior to energy minimization, RMSD calculation between the two conformations for the heavy atoms of residues 1−3 yields a large value of 7.9 Å.

3.3. Effects of N-Terminus and Nucleotide Substitutions. Recalculation of the binding energies for the unsolvated actin−ADP structure with the extended N-terminal conformation reveals that all calcium ions, save for the calcium at binding site CA384, have binding energies comparable to those obtained for 1J6Z actin with the N-terminus appended from 1ATN. The calcium binding energy at the CA384 site, which is the closest site to the N-terminus of the actin monomer, is 30 kcal/mol higher when the residues added using the extended method. Simulation snapshots indicate that the sequence of negatively charged residues 1−4 at the N-terminus do not approach the calcium at CA384 as closely if the initial configuration selected for MD simulation is the extended rather than the 1ATN configuration for the N-terminus. This result underscores the importance of selecting the most physically realistic initial coordinates for the protein structure based upon full utilization of available crystallographic data.

In the polymerized actin filament, the nucleotide site is occupied by ADP, whereas in monomeric actin ATP is more physiologically relevant because it selectively binds to the monomer as a precursor to ATP hydrolysis during filament assembly. Calcium binding energies are reported in Table 1 for in vacuo actin with ATP substituted for ADP in the monomer cleft. It is observed that the binding energies of all calcium ions bound to actin−ATP are similar to those bound to actin−ADP. The largest difference when the nucleotides are substituted occurs, unsurprisingly, at CA382, the calcium site located adjacent to the nucleotide binding site. From MD simulations of actin−ATP, the electrostatic interaction of the calcium located at CA384 with the nucleotide is −750 kcal/mol; in actin−ADP, the calcium−nucleotide interaction is −550 kcal/mol, or 200 kcal/mol weaker. This decrease is partially compensated by the stronger electrostatic interaction between the calcium bound at CA382 and Asp-154 in the actin−ADP system. The interaction between this residue and the calcium at CA382 increases by 140 kcal/mol relative to the same interaction for the actin−ATP system. The net increase in the calcium binding energy at the CA382 site in actin−ATP, relative to actin−ADP is therefore a more modest 60 kcal/mol. Calcium ions bound at the other actin sites are sufficiently far removed from the nucleotide so that there is little difference in their binding energies for ADP or ATP, even though ATP bears an additional negative charge (i.e., $-3e$ vs $-4e$).

3.4. Effect of Calcium Loading. The contribution of calcium−calcium repulsion toward the binding potential energy of calcium on an actin monomer fully loaded with calcium ions may be evaluated for unsolvated actin−ADP by comparing the values of ΔE in Table 1 when ion−ion repulsion is included and excluded. In the former case, the binding potential energies of all calcium ions are substantially higher (i.e., less negative) because of the long-range electrostatic repulsion between the divalent cations. The difference when the calcium ion pair repulsions are included and excluded averages 223 kcal/mol for the six calcium ions. Binding potential energies in Table 1 have been calculated for the six-calcium actin−ADP system with ion−ion repulsion neglected as an estimate of the binding potential energy for calcium adsorption onto a monomer that is unoccupied by other calcium ions. The reported energy, per Figure 2d, is that due to the interactions of the bound calcium ion with the protein, nucleotide and water only. In a rigorous calculation of the binding energy from the one-calcium actin−ADP system, the potential energy change would presumably be higher (i.e., less negative) because of exchange of calcium with at least one potassium ion that would likely occupy the calcium affinity site. So, the binding potential energies reported in Table 1 must be considered as only an approximation of ΔE for calcium adsorption onto an unbound (i.e., calcium-free) actin monomer.

Recognizing this caveat, the energies reported in Table 1 are nonetheless useful for assessing the relative magnitude of protein−ion interactions for the actin monomer, and, assuming calcium adsorption on actin is enthalpically driven, for rank-ordering the affinities of the calcium binding sites at low calcium loadings. In this regard, calcium site CA382 has the strongest affinity for calcium ion binding at low free calcium concentration, according to the calculations for the unsolvated monomer. CA384 has the next highest affinity (i.e., the next-lowest binding potential energy change), followed by CA383, CA385, and CA386, which all have comparable binding energies. For the unsolvated actin monomer, site CA387 binds calcium much more weakly than the other five crystallographic sites identified in the 1J6Z PDB structure. Interestingly, for the fully loaded, unsolvated monomer, for which calcium−calcium repulsion is the most significant, the binding energy of site CA384 near the actin N-terminal region slightly exceeds the binding energy of the nucleotide-associated site CA382, which is the preferred calcium binding site at low free calcium concentrations.

3.5. Effect of Solvation Layer Thickness. To investigate the effect of solvation of the actin monomer on calcium binding energies, MD calculations were performed with the protein solvated in a 10-Å shell of water molecules. Global and subset RMSDs for the solvated actin monomer are shown in Figure 4b. The RMSDs for all components of the system except ADP are considerably smaller than the corresponding RMSDs for the in vacuo system reported in Figure 4a. This is expected because ADP is in the cleft region and is thus largely screened from the solvent shell. In other regions near the protein outer surface, solvent water stabilizes the system and to some extent restrains movement of the protein side chains and calcium ions. Even the RMSD for intracrystalline water decreases to 1.90 Å in the solvated system after 1 ns of MD simulation.

Solvation strongly affects the binding energies of the calcium ions, as indicated in Table 1. Although site CA382 still binds calcium the most strongly of the crystallographic calcium sites, the binding potential energies of the other five crystallographic sites are brought into approximate parity in the presence of solvent. Additional insight is obtained by examining MD

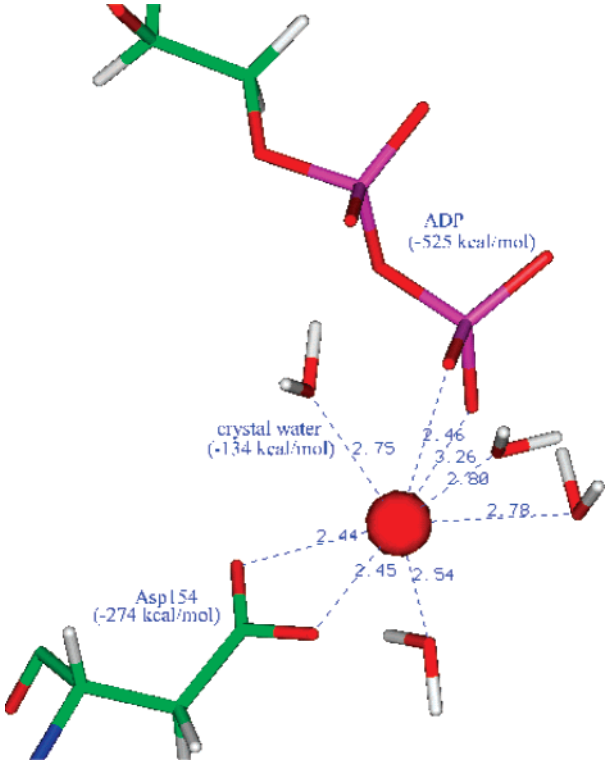

Figure 7. Coordination of CA382 binding site from MD simulation snapshot taken at 430 ps. Side chains, ADP, and water molecules within a distance of 3.5 Å from the calcium ion are shown. The red sphere is the calcium ion; the red, white, green, blue, and violet segments represent oxygen, hydrogen, carbon, nitrogen, and phosphorus atoms, respectively, in the amino acid side chains, ADP, and water molecules. Distances between the calcium ion and the coordinating oxygen atoms are reported in angstroms. The same description and color scheme applies the binding sites for the other calcium ions shown in Figures 8−12.

snapshots of the coordination of the calcium ions at the six binding sites, presented in Figures 7−12. For each calcium ion, the principal contributions to the binding energy are electrostatic interactions with the carboxyl oxygens of one or two nearby acidic residues (or the case of CA382, the phosphate oxygens of ADP) and with three or four intracrystalline or solvent water molecules. For two calcium sites, CA384 and CA387, solvation changes the binding site coordination significantly. For CA384, intrusion of solvent water reduces its interactions with Gln-354, and in part contributes to a decrease in its calcium binding energy. Conversely, calcium binds more strongly at surface site CA387 in the solvated monomer because of an increase in the partial hydration shell at this site.

As shown in Table 1, MD simulations performed with a 15-Å shell of 5198 solvent water molecules yielded calcium binding energies that are similar to the results obtained for the 10-Å solvation layer of 3502 water molecules, with a mean difference in binding potential energy of 3.3% for the six ions, and even closer agreement for the two different layer thicknesses if the anomalously large difference for CA386 is discounted. Thus, a 10-Å solvation layer appears to be sufficient for evaluating the effect of solvation on calcium site binding energies, although far-field electrostatic interactions of the system constituents should also be included, as considered in the next section.

In Table 2, the binding potential energy is reported for calcium ion adsorption on the actin−ADP monomer solvated with a 10-Å water layer, using the extended electrostatics model[23] to include charge interactions between spatially distant regions of the protein, ligands and water. The calcium binding

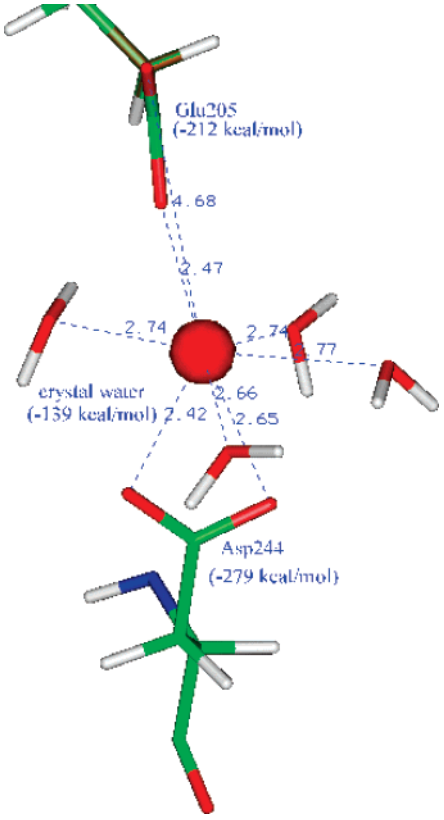

Figure 8. Coordination of CA383 binding site.

energies for the actin−ADP system with explicit solvation and extended electrostatics differ from those reported in Table 1 for the solvated monomer without far-field interactions. In comparing the values for ΔE when the calcium pair repulsion contributions are removed, it is found that the binding potential energy decreases on average by nearly 100 kcal/mol when extended electrostatics are included in the MD simulation. From analysis of molecular simulation snapshots, it was found that this energy decrease can be partially attributed to a closer proximity of coordinating water molecules to the calcium ions in their binding sites. Irrespective of these differences, CA382 remains the site with the highest affinity for calcium binding when extended electrostatics are included. For the other five calcium binding sites, the binding potential energies are statistically indistinguishable when ion−ion repulsions are included in the calculation. Hence, the affinities of these sites all appear to be comparable for adsorption of a sixth calcium ion, when the other five sites are already occupied by calcium ions. At low calcium loadings, when calcium pair repulsion is less-significant, more differentiation is observed between the site affinities. Sites CA386 and CA387 emerge as the sites with the next second- and third-highest affinities, followed by CA383 and CA385, which have statistically equivalent binding free energies. CA384 binds most weakly among of the six sites at low calcium loadings.

3.6. Effect of Periodic Boundary Conditions. The results presented thus far are based upon MD simulations for an isolated solvated actin monomer. Using periodic boundary conditions, boundary effects on calcium ion binding were considered for two limiting cases: at high free calcium ion concentrations, wherein each actin monomer is fully loaded with six calcium ions, and calcium ion pair repulsions are included; and at low free calcium ion concentrations, wherein the actin monomers are unbound and calcium pair repulsions are neglected. In the former scenario, the fully bound monomer is charge-neutral; whereas in the latter, the unbound monomer bears a net charge of $-12e$. For the periodic system at high calcium loadings, the binding energy of the calcium ion is given as the sum of its interactions with the $(N - 1)$ other atoms in the primary cell and the $(N - 1)(M - 1)$ atoms in the $(M - 1)$ image cells (ignoring the interaction of the calcium ion with its own image). At low calcium loadings, the same summation is involved, but with $(N - 6)$ atoms in the primary cell and in each periodic image cell. Binding free energies calculated by explicit summation of the energies in the $3 \times 3 \times 3$ periodic system ($M = 27$) and the $5 \times 5 \times 5$ periodic system ($M = 125$) are shown in Table 3. At low calcium loadings, each image cell bears a net negative charge of $-12e$, and so the calcium ion binding energies increase as M increases due to the long-ranged electrostatic interactions, whereas at high loadings, the image cells have a zero net charge and so the calcium binding energies do not increase with M. For both low and high calcium loadings, the CA382 binding site exhibits the highest affinity for calcium in the periodic system. Binding energies for all affinity sites at high loadings (i.e., when calcium ion pair repulsion is included) in the periodic systems are comparable to the binding energies reported in Table 2 for the isolated ($M = 1$), solvated, fully bound monomer. At low calcium loadings in the periodic system, the CA382 site consistently binds calcium most strongly, with an affinity 50−00 kcal/mol greater than the other binding sites. This difference is comparable to the binding energy differences between CA382 and the other sites shown in Table 2 for the nonperiodic system. Hence, although the total binding energies computed at low calcium loadings depend on the number of periodic images included in the calculation, the relative differences in the binding potential energies of the calcium affinity sites are found to be the same, irrespective of the periodicity of the system.

3.7. Free Energies for Binding on Actin. The relative binding free energy was estimated from the thermodynamic cycle shown in Figure 3 using trajectories from MD simulations with PBCs and the Ewald summation. In principle, one should use the MD trajectory of the complex system composed of a single calcium ion and the protein to compute the relative binding free energy. In this study, the MD trajectory for the complex system composed of six calcium ions bound to actin was used to approximate the relative binding free energies for the one-ion system. Twenty conformations were collected from the MD trajectory at 10-ps intervals following equilibration. Intracrystalline water and solvent water molecules were removed from these conformations, and ΔG_{solv}^{elec} and ΔE_{gas} were calculated using the Poisson−Boltzmann equation. The values obtained for ΔG_{solv}^{elec} from the 20 conformations were consistent to within approximately 1%, whereas the computed values for ΔE_{gas} varied between 2% and 7% for the calcium affinity sites using the sampled conformations. Assigning the ensemble average of the sum of ΔG_{solv}^{elec} and ΔE_{gas} as the binding free energy, and using the summation of $<\Delta G_{solv}^{elec}>$ and $<\Delta E_{gas}>$ for affinity site CA382 as a reference, binding free energies relative to CA382 were computed for the other affinity sites on the actin monomer (Table 4). Binding site CA382 clearly exhibits the highest binding affinity when the polarizability of the ion−protein complex is taken into account by assigning a dielectric constant of 4−20. In contrast, for a dielectric constant of unity, the CA382 site has a slightly lower affinity than the CA385 site, and all six sites are roughly comparable in their binding energies. It is thus important to consider the polarizability of the protein when computing the binding free energy using the continuum electrostatics model. Indeed, Antosiewicz

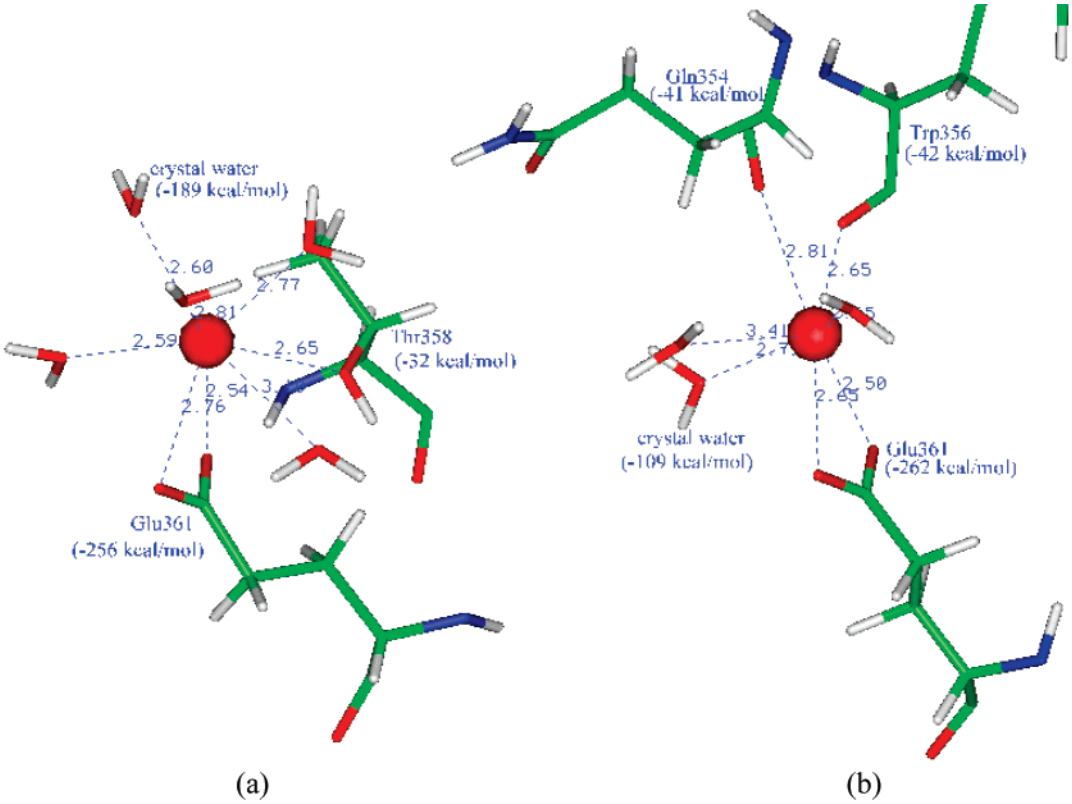

Figure 9. Coordination of CA384 binding site (a) without and (b) with solvent water.

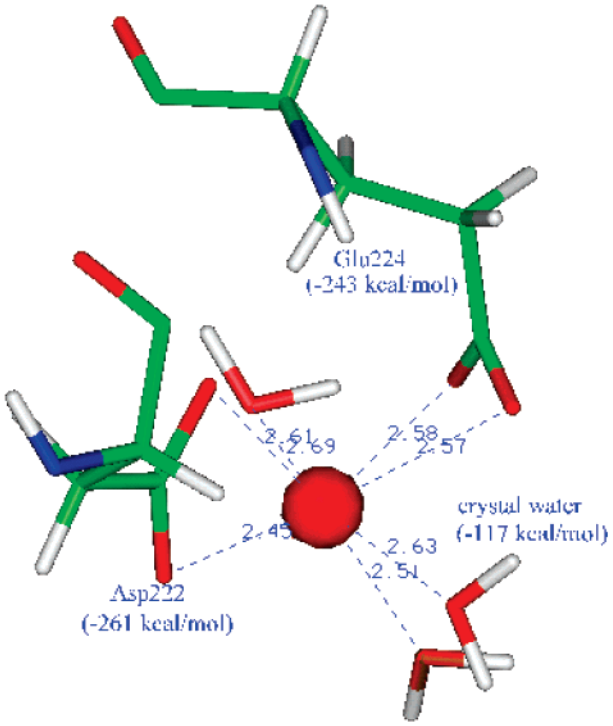

Figure 10. Coordination of CA385 binding site.

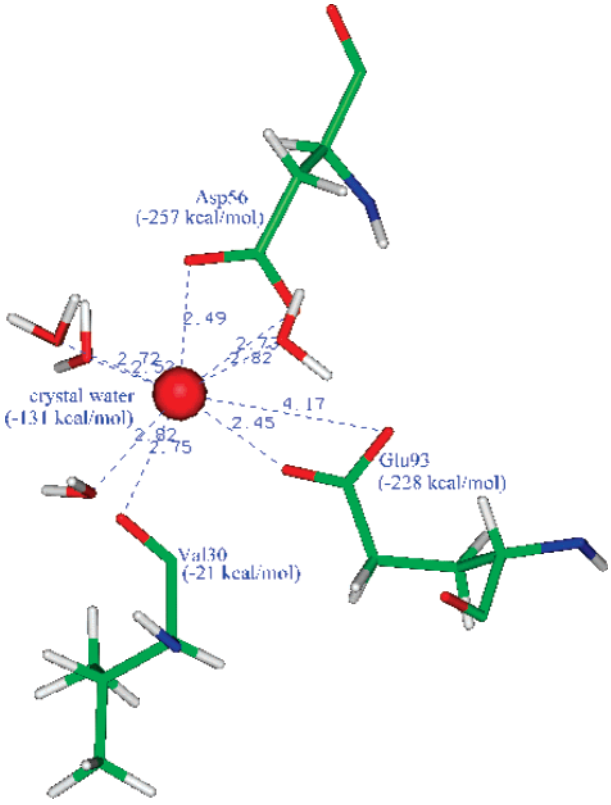

Figure 11. Coordination of CA386 binding site.

et al.[37] have suggested using an internal protein dielectric constant of 20. They have reasoned that a high dielectric constant compensates for omission of local conformational changes and specific ion binding.

We have studied the sensitivity of the grid size to the binding free energy by setting the grid size to 0.5 Å. The relative binding free energies shown in Table 4 vary only by about 1−2 kcal/mol. This justifies that the grid size of 0.4 Å used in the calculation is small enough to get good estimates of the relative binding free energy.

3.8. Exchange of Cations at Actin Affinity Sites. For the CA382 binding site in the cleft region of the actin monomer, the free energy change for Zn^{2+}−actin → Ca^{2+}−actin was calculated from the perturbation method as 92.8 kcal/mol,

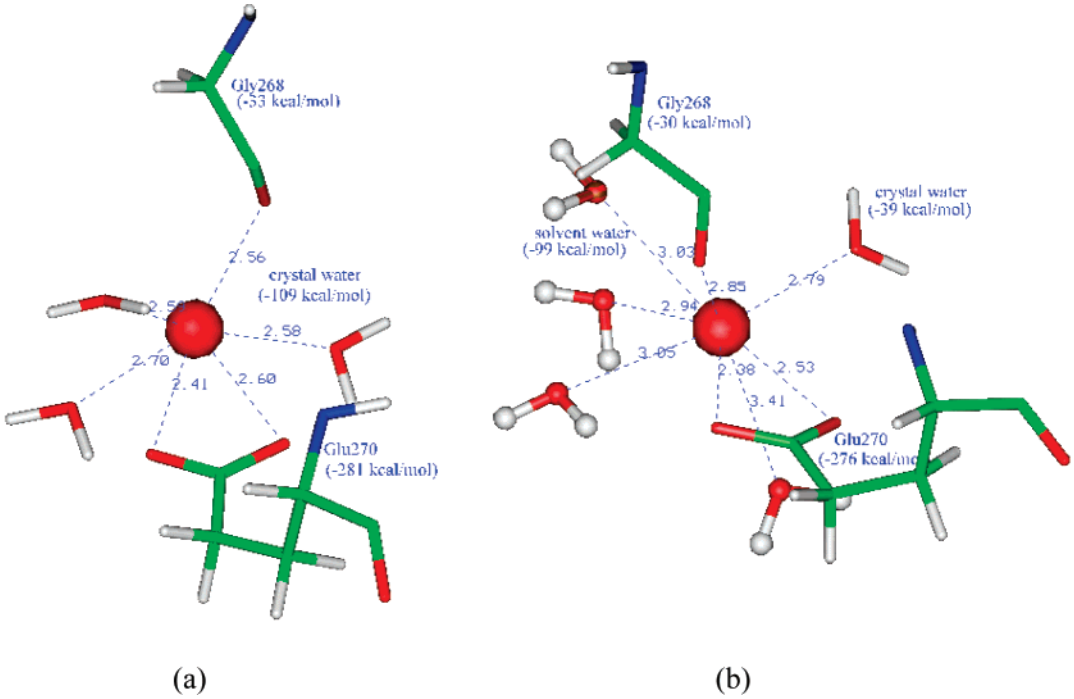

Figure 12. Coordination of CA387 binding site (a) without and (b) with solvent water.

TABLE 2: Potential Energy Differences ΔE Obtained from MD Simulation with Extended Electrostatics for Calcium Binding on the Solvated Actin−ADP System with Six Bound Calcium Ions and a 10-Å Shell of Solvent Water[a]

	ΔE (kcal/mol)	
Ca-Ca repulsion	yes	no
CA382	−692 (19)	−962 (19)
CA383	−669 (17)	−878 (17)
CA384	−668 (17)	−836 (17)
CA385	−673 (18)	−872 (17)
CA386	−667 (18)	−911 (19)
CA387	−670 (19)	−894 (19)

[a] Inclusion or neglect of calcium−calcium repulsion in the energy calculation is noted. Standard deviations for the reported values are enclosed in parentheses.

TABLE 3: Potential Energy Differences ΔE Obtained from MD Simulation for the Periodic Solvated Actin−ADP System, with Six Bound Calcium Ions Per Monomer, and Periodic Arrays of Dimension 3 × 3 × 3 and 5 × 5 × 5, Containing $M = 27$ and $M = 125$ Image Cells, Respectively[a]

	ΔE (kcal/mol)			
Ca-Ca repulsion	no		yes	
M	125	27	125	27
CA382	−7140 (15)	−3019 (15)	−692 (19)	−692 (19)
CA383	−7002 (28)	−2880 (28)	−672 (26)	−672 (26)
CA384	−7020 (16)	−2900 (16)	−686 (18)	−686 (18)
CA385	−6993 (18)	−2872 (18)	−626 (21)	−626 (21)
CA386	−7102 (20)	−2980 (20)	−680 (20)	−680 (20)
CA387	−7014 (17)	−2893 (17)	−621 (25)	−621 (25)

[a] Inclusion or neglect of calcium−calcium repulsion in the energy calculation is noted. Standard deviations for the reported values are enclosed in parentheses.

whereas for Ca^{2+}−actin → Zn^{2+}−actin, a free energy change of −86.0 kcal/mol was obtained. The free energy change for Zn^{2+}−actin → Ca^{2+}−actin is thus estimated to be 89.4 (3.4) kcal/mol. Taking into account the solvation energies of the unbound calcium and zinc ions, the free energy change for

$$Ca^{2+} + Zn^{2+}\text{−actin} \rightarrow Zn^{2+} + Ca^{2+}\text{−actin}$$

TABLE 4: Binding Free Energies from the Poisson−Boltzmann Equation, Relative to the CA382 Site, for Different Dielectric Constants for Calcium Binding onto an Unbound Actin Monomer at the Six Affinity Sites

	relative binding free energy (kcal/mol)		
binding site	$\epsilon = 1$	$\epsilon = 4$	$\epsilon = 20$
CA382	0	0	0
CA383	11.6	123.9	206.5
CA384	13.3	87.8	105.7
CA385	−13.7	73.2	96.8
CA386	9.2	78.3	109.1
CA387	1.8	117.7	173.9

is calculated as −12.3 kcal/mol. Hence, calcium will displace zinc ion at the CA382 binding site in the actin monomer cleft region. The MD simulations further indicate that binding site CA382 exhibits the highest binding affinity for calcium. This is consistent with experimental measurements of divalent cation binding affinities for monomeric actin that indicate a preference for calcium binding over zinc at the highest affinity site.[1,17,18]

4. Discussion

The MD simulations from all model calculations show that the CA382 site near ADP in the actin monomer cleft region consistently has the highest calcium affinity of the six crystallographic calcium binding sites, as measured in terms of its binding potential energy and binding free energy. The other sites, CA383−CA387, presumably serve as the so-called intermediate affinity binding sites for calcium adsorption, with comparable binding energies measured for these sites on the fully loaded actin monomer in the solvated system. The simulation results are consistent with experimental characterization of actin affinity sites for calcium adsorption, which identified one tight-binding site and four adsorption sites of lower, and approximately equal, affinity.

The rank ordering of the binding energies of the calcium sites is not sensitive to the type of nucleotide bound to actin; however, it does depend strongly on the presence or absence of solvent water. From experimental measurement, it is known that five

divalent cations must bind to the actin monomer before it can polymerize into filaments. The vacuum MD simulation results suggest that site CA387 would be left vacant in favor of calcium loading at the other five affinity sites during actin filament self-assembly. However, MD simulations of the solvated monomer using the extended electrostatics and the PBC with Ewald summation models indicate that the binding energies of sites CA383−CA387 are statistically indistinguishable. No conclusive statement can therefore be made regarding which four of the five binding sites are occupied at the onset of actin polymerization, if in fact a unique set of calcium binding coordinates exists. It is possible that steric and energetic analyses of the calcium binding sites on filamentous actin may answer this question. Three of the sites, CA383, CA385, and CA387, lie within domain II of the actin monomer. This domain faces inward toward the central axis of the helical filament, and it has several contacts with adjacent monomer units in surface regions close to the aforementioned calcium binding sites. It is thus possible that one of the domain II calcium sites may be excluded on the basis of steric interference or unfavorable energetics in polymerized filamentous actin.

Juffer and Vogel calculated the effect of calcium ion binding on the pK_a values of Calbindin residues.[38] They found that calcium binding lowers the pK_a values for all titrating sites to varying degrees, with residues closer to the calcium binding sites predictably more affected than those further removed. In this work, the charge states for all amino acid residues were set to zero, save for the +1 charges assigned to Arg and Lys residues and the −1 charges assigned to Asp, Glu, and four His residues (as noted in the Methods section). It is reasonable to expect that calcium binding similarly effects a pK_a shift for proximate residues of the actin monomer, and this shift may in turn affect the binding free energies of the calcium ions on the affinity sites. Assessment of these possible pK_a shifts is a worthwhile subject to undertake in a future study of calcium ion binding on the actin monomer. The results reported in the present work confirm, to a first order of approximation, experimental observations of calcium binding to monomeric actin.

Acknowledgment. We thank the W. M. Keck Foundation for financial support of this work. A computing cluster equipment grant provided by Sun Microsytems is also gratefully acknowledged.

References and Notes

(1) Sheterline, P.; Clayton, J.; Sparrow, J. C. *Actin*, 4th ed.; Oxford University Press: New York, 1998.

(2) Oda, T.; Makino, K.; Yamashita, I.; Namba, K.; Maeda, Y. In *Molecular Interactions of Actin*; dos Remedios, C. G., Thomas, D. D., Eds.; Springer-Verlag: Berlin, 2000; pp 43−58.

(3) Dos Remedios, C. G.; Moens, P. J. *Biochim. Biophys. Acta* **1995**, *1228*, 99−1224.

(4) De La Cruz, E. M. In *Molecular Interactions of Actin*; dos Remedios, C. G., Thomas, D. D., Eds.; Springer-Verlag: Berlin, 2000; pp 122−134.

(5) Jamney, P. A.; Shah, J. V.; Tang, J. X.; Stossel, T. P. In *Molecular Interactions of Actin*; dos Remedios, C. G., Thomas, D. D., Eds.; Springer-Verlag: Berlin, 2002; pp 181−199.

(6) Chik, J. K.; Lindberg, U.; Schutt, C. E. *J. Mol. Biol.* **1996**, *263*, 607−623.

(7) Kabsch, W.; Mannherz, H.; Suck, D.; Pai, E.; Holmes, K. C. *Nature* **1990**, *347*, 37−44.

(8) Lorenz, M.; Popp, D.; Holmes, K. C. *J. Mol. Biol.* **1993**, *234*, 826−836.

(9) Otterbein, L. R.; Graceffa, P.; Dominguez, R. *Science* **2001**, *293*, 708−711.

(10) Estes, J. E.; Selden, L. A.; Kinosian, H. J.; Gershman, L. C. *J. Muscle Res. Cell Motil.* **1992**, *13*, 272−284.

(11) Kinosian, H. J.; Selden, L. A.; Estes, J. E.; Gershman, L. C. *J. Biol. Chem.* **1993**, *268*, 8683−8691.

(12) Strzelecka-Golaszewska, H. In *Molecular Interactions of Actin*; dos Remedios, C. G., Thomas, D. D., Eds.; Springer-Verlag: Berlin, 2000; pp 23−41.

(13) Strzelecka-Golaszewska, H.; Prochniewicz, E.; Drabikowski, W. *Eur. J. Biochem.* **1978**, *88*, 219−227.

(14) Strzelecka-Golaszewska, H.; Prochniewicz, E.; Drabikowski, W. *Eur. J. Biochem.* **1978**, *88*, 229−237.

(15) Selden, L. A.; Estes, J. E.; Gershman, L. C. *J. Biol. Chem.* **1989**, *264*, 9271−9277.

(16) Carlier, M. F.; Pantaloni, D.; Korn, E. D. *J. Biol. Chem.* **1986**, *261*, 10778−10784.

(17) Strzelecka-Golaszewska, H. *Biochim. Biophys. Acta*. **1973**, *37*, 60−69.

(18) Strzelecka-Golaszewska, H.; Boguta, G.; Zmorzynski, S.; Moraczewska, J. *Eur. J. Biochem.* **1989**, *182*, 299−305.

(19) Wriggers, W.; Schulten, K. *Biophys. J.* **1997**, *73*, 624−639.

(20) Yao, X. Y.; Grade, S.; Wriggers, W.; Rubenstein, P. *J. Biol. Chem.* **1999**, *274*, 37443−37449.

(21) Brooks, B. R.; Bruccoleri, R. E.; Olafson, B. D.; States, D. J.; Swaminathan, S.; Karplus, M. *J. Comput. Chem*. **1983**, *4*, 187−217.

(22) Jorgensen, W. L.; Chandrasekhar, J.; Madura, J. D.; Impey, R. W.; Klein, M. L. *J. Chem. Phys.* **1983**, *79*, 926−935.

(23) Stote, R. H.; States, D. J.; Karplus, M. *J. Chem. Phys.* **1991**, *88*, 2419−2433.

(24) Keseru, G.; Kolossvary. I. *Molecular Mechanics and Conformational Analysis in Drug Design*; Blackwell Science: Oxford, 1999.

(25) Noskov, S. Y.; Lim, C. *Biophys. J.* **2001**, *81*, 737−750.

(26) Sitkoff, D.; Sharp, K. A.; Honig, B. *J. Phys. Chem.* **1994**, *98*, 1978−1988.

(27) Honig, B; Nicholls, A. *Science* **1995**, *268*, 1144−1149.

(28) Roux, B. *Biophys. J.* **1997**, *73*, 2980−2989.

(29) Essmann, U.; Perera, L.; Berkowitz, M. L.; Darden, T.; Lee, H.; Pedersen, L. G. *J. Chem. Phys.* **1995**, *103*, 8577−8593.

(30) Gmelin Institute *Handbuch der Anorganischen Chemie 8 Auflage*; Springer, Ger: Berlin, 1956.

(31) Pogue, R.; Atkinson, G. *J. Solution Chem.* **1989**, *18*, 249−264.

(32) Burgess, J. *Metal Ions in Solution*; John Wiley & Sons: New York, 1978

(33) Liang, J.; Edelsbrunner, H.; Woodward, C. *Protein Sci.* **1998**, *7*, 1884−1897.

(34) Liang, J.; Dill, K. A. *Biophys. J.* **2001**, *81*, 751−766.

(35) Aikio, J.; Mahonen, P. *Astron. J.* **1998**, *497*, 534−540.

(36) Stavrev, K. Y. *Astron. Astrophys., Suppl. Ser.*; **2000**, *144*, 323−347.

(37) Antosiewicz, J.; McCammon, J. A.; Gilson, M. K. *J. Mol. Biol.* **1994**, *238*, 415−436.

(38) Juffer A. H.; Vogel, H. J. *Proteins* **2000**, *41*, 554−567.